航測及遙測學刊 第十九卷 第3期 第207-224頁 民國104年01月
Journal of Photogrammetry and Remote Sensing
Volume19, No3, January 2015, pp. 207-224

Surface deformation of the central Taiwan and its tectonic implication of the PSI analysis

Ting-Hsuan Hsu [1*] Chung-Pai Chang [2*] Wu-Lung Chang [3]

ABSTRACT

The Puli Basin, located between the Western Foothills and the Hsüehshan Range is the largest basin in the active orogeny in central Taiwan. South to the Puli Basin, a series of small basins spread along the NNE direction. Various tectonic models have been proposed in previous studies to interpret the formation of the Puli Basin. In this study, we aim to measure the deformation and to understand the tectonics of Puli Basin by the method of satellite remote sensing and field observation. We applied the Persistent Scatterer Interferometric SAR technique to monitor the surface deformation. Our result shows a relative lower LOS velocity in Puli Basin, which implies the change of depth of the subsurface basal detachment. A steep ramp along the detachment is proposed for the grown structure underneath the Puli Basin in this study. In order to interpret the mechanism of surface deformation in central Taiwan, we implement several forward models based on previous researches and our interferometric results and then compare our observations with accurate GPS and precise leveling data. These results can be compared with our field observations and with the recent seismicity data (20130327 and 20130602) to examine the activity and geometry of faults of this area, where a conjugate fault system below the basins was suggested. Due to the lack of evidence, the relationship between the conjugate system and the basin subsidence mechanism is hard to determine but may be the key to understand the tectonic activity in central Taiwan.

Keywords: active tectonics, Puli Basin, Persistent Scatterer Interferometric SAR, dislocation model, field observation

1. Introduction

Taiwan is formed due to the convergence between the Eurasian plate and Philippine Sea plate, resulting into compression-dominated stress building up high mountains. In general, the Taiwan mountain belt is divided into five NNE trending geologic provinces. From west to east these zones are: the Coastal Plain, the Western Foothills, the Hsüehshan Range, the Central Range, and the Coastal Range (Ho, 1982, 1986) (Figure 1). In between these high mountain ranges there are several inter-mountainous basins in the southern Hsüehshan Range, and Puli Basin is the largest one. These inter-mountainous basins are all formed along the strike of the major NNE trending geologic provinces of this area.

However, the development of the basins is still a mystery due to widely varied views from previous researches. Based on those studies, five main theories have been put forward, which are listed as follows: (1) bedrock down warping (Hayasaka, 1930, in Japanese; Tomita, 1953, in Japanese; Huang, 2008, in Chinese; Ke, 2009, in Chinese), (2) pull-apart basin caused by transtension of strike-slip fault (Biq, 1989), (3) movement of basal detachment under basins (Chen *et al*., 2001), (4) piggyback basin in the fold-and-thrust belt (Chu, 1991, in Chinese; Mueller *et al*., 2002; Powell *et al*., 2002), (5) basins resulted from transpression and transtension (Chen, 2003, in Chinese). Numerous measuring techniques have been applied to study this area such as, borehole data (Chen, 1978, in Chinese), geodesy (global positioning system, GPS) (Chen *et al*., 2001), aerial photography (Chen, 2003, in Chinese), balance cross section (Yue *et al*., 2005), geomorphic analyses (Yang *et al*., 2007, in Chinese), reflection seismology (Huang, 2008, in Chinese; Ke, 2009, in Chinese), gravity anomaly measurements (Ke, 2009, in Chinese),

[1] Research Assistent, Department of Earth Sciences, National Central University
[2] Professor, Center for Space and Remote Sensing Research, National Central University
[3] Associate Professor, Department of Earth Sciences, National Central University
*Corresponding Author, Phone: 886-3-4227151 ext. 57627, E-mail: cpchang@csrsr.ncu.edu.tw
Received Date: Nov. 08, 2013
Revised Date: Aug. 17, 2014
Accepted Date: Aug. 27, 2014

optically stimulated luminescence (OSL) dating (Yanites *et al*., 2010), and field investigation (e.g., Brown *et al*., 2012).

In this study, we applied the Persistent Scatterer Interferometric Synthetic Aperture Radar (PSI), an advanced technique developed by Hooper *et al*. (2004), to obtain new insights into the present-day deformation pattern of the Central Taiwan. So far, this technique has successfully been applied on tectonic analysis for detecting the subtle ground deformation (up to 1~2 mm/year) (e.g., Hooper *et al*., 2004; Chang *et al*., 2010). Our PSI result shows an obvious subsidence occurring in the basins. The apparent change of the movement might relate to the effect of the neighboring structures. Therefore, understanding the features of the underground structures is a top priority in our research. Additionally, we compare our InSAR observations with other geodetic measurements such as the accurate GPS and precise leveling data for a concrete conclusion and a more reliable result.

In order to understand the relationship between the fault movement and the corresponding surface deformation, we implement Coulomb 3.3 software (Toda *et al*., 2005; Lin *et al*., 2004) to model the ground effect resulting due to movement along the faults. Moreover, a series of earthquake has occurred in Nantou area, which may be due to the ongoing basal detachment stretching eastward. We investigate the outcrops and also the kinematic indicators of the faults in the epicenter area, and it helps us to understand the structural activity within this region.

2. Geological Background

The inter-mountainous basins partly infill a region of lower topography, lying between the Peikang River and the Choshui River, which is located at the edge of the slate belt in the southern Hsüehshan Range in central Taiwan (Figure 2). From north to south, there are about five basins, namely Puli, Yuchi, Sun-Moon Lake, Touche, and Chongkuei covering a distance of about 30 km. All these basins are formed along the strike of the major NNE-SSW trending faults.

Structurally, Central Taiwan is considered to be a typical fold-and-thrust belt, and a feature of the active foreland fold-and-thrust belts is the presence of a horizontal basal surface of detachment or décollement, which dips toward the interior of the mountain belt. (e.g., Chapple, 1978; Davis *et al*., 1983; Stockmal, 1983;Suppe, 1983; Dahlen *et al*., 1984). Typically, the basal detachment lies in weak shale or evaporite at or near the basement. Rocks below this gliding plane are autochthonous, while rocks above are allocthonous (Van Der Pluijm *et al*., 2004), which results in large deformation such as the imbricate faults, numerous folds and the inter-mountainous basins and makes this region so complex. A series of west-vergent, NNE-striking thrusts nearly perpendicular to the direction of tectonic stress are found in the central Taiwan. From west to east are: the Changhua fault, Chelungpu fault, Shuangtung fault, Shuilikeng fault, Meiyuan fault, Tili fault and the Lishan fault (Figure 2).

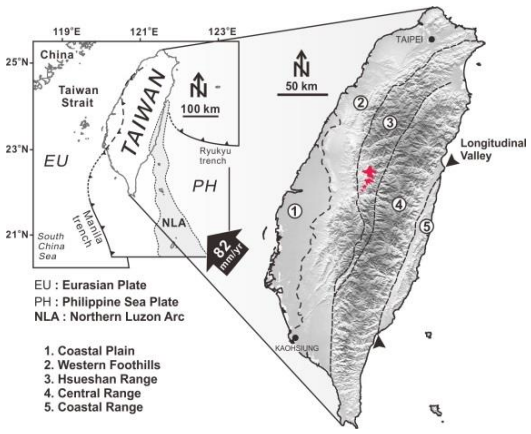

Figure 1 Topography and the tectonic setting of Taiwan (modified from Chang *et al*., 2009). Taiwan is divided into six roughly N-S oriented tectonostratigraphic zones that are separated by major faults. From west to east they are Coastal Plain, the Western Foothills, the Hsüehshan Range, the Central Range, and the Coastal Range. Red color shows the position of the basins.

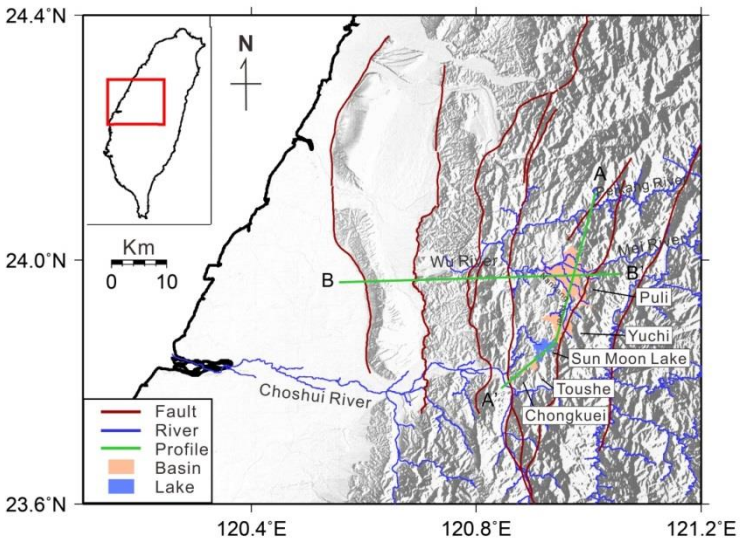

Figure 2 The topography and the structure of our study area. Blue lines show the river systems, and red lines are the faults. Green lines are the location of the N-S profile and E-W profile. From the west to the east, the main NNE-striking thrusts are the Changhua fault, Chelungpu fault, Shuangtung fault, Shuilikeng fault, Meiyuan fault, Tili fault and the Lishan fault.

3. Research results

An advanced technique, Persistent Scatterer InSAR (PSI) developed by Hooper *et al*. (2004), has improved the conventional InSAR by a characteristic to identify and isolate the stable pixels generally referred as PS pixels. The main propose for this new method is the episodic crustal deformation analysis in non-urban regions. Hooper *et al*. (2004) suggested that if a pixel is dominated by one stable scatterer that is brighter than the background scatterers, the variance of phase is thought to be relative lower than the rest, and may be the idea information to understand the real deformation. In this study, the results are divided into two parts: interferometric results and dislocation model. According to our surface observation from PSI, we consider the possibilities of fault movement underground by dislocation model. The details are discussed below.

3.1 Interferometric results

We applied StaMPS (Stanford Method for PS) to process the SAR image acquired by ERS and Envisat satellites in descending orbit over central Taiwan (Figure 3b, track: 232; frame: 3123). The systems in this study are right side-looking spaceborne radar with a look angle about 23°.

In order to avoid the coseismic effect of the Chi-Chi earthquake (21 Sep. 1999), we collected 41 ERS images from October 1993 to August 1999 and 21 Envisat images from June 2004 to September 2008, considering the background tectonic effects only.

Although the higher accuracy of the DEM reduces the ambiguity in the displacement estimation step, the accuracy of the estimated deformation signal improves as the number of interferogram increase (at least >12). Therefore, the accuracy of the DEM is not usually important in the PS processing (Hooper et al., 2007), and the number of the images are sufficient in our study. In order to optimize our observation results, we chose a master image with minimum decorrelation, i.e., the one has shortest perpendicular baseline and relatively short time interval with the slaves (Hooper et al., 2007). The data sets are shown in Table 1 and Table 2. We produced 40 interferograms from ERS and 20 interferograms from Envisat and displayed them as time series of displacement (Figure 3a and Figure 4). All the images are shown with a relative LOS displacement to the master one, 19970605 for the ERS and 20070906 for the Envisat.

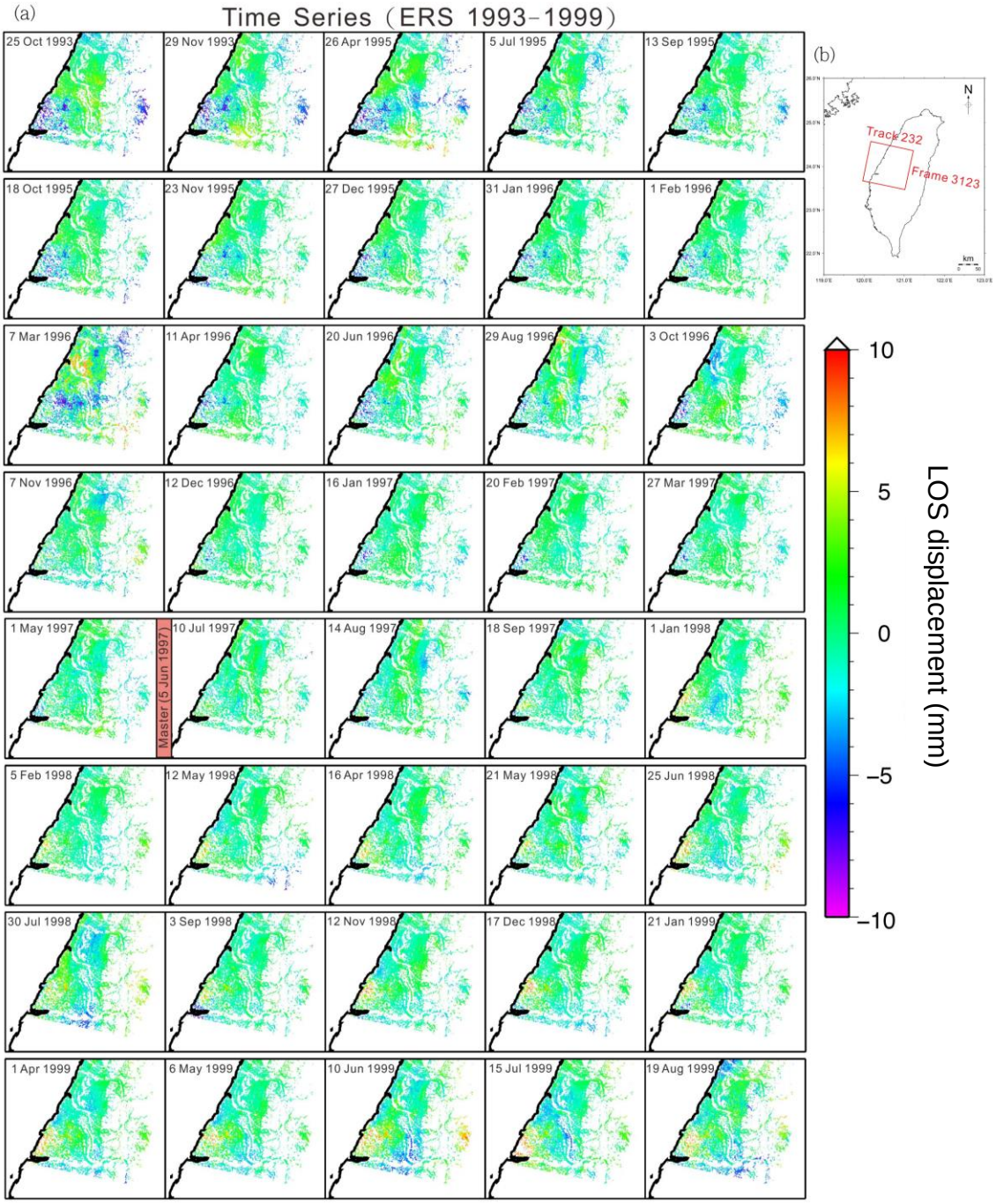

Figure 3 (a) 41 ERS images are used in our study. Displacements are given relative to PS pixels on 5 June 1997 (master image). Before the Chi-Chi earthquake on 21 Sep. 1999, the surface deformation does not show an obvious change in central Taiwan. (b) Satellites orbit in central Taiwan (track: 232; frame: 3123).

Table 1 Interferometric data used from ERS satellite (1993-1999). Blue color indicates the master image

Date	Time interval (day)	Baseline (m)
19931025	-1319	864.6
19931129	-1284	811.5
19950426	-771	-55
19950705	-701	-567
19950913	-631	-508
19951018	-596	1172.8
19951123	-560	-624.9
19951227	-526	899.6
19960131	-491	464.7
19960201	-490	575.8
19960307	-455	655.8
19960411	-420	475.1
19960620	-350	-61.6
19960829	-280	-395.9
19961003	-245	-82
19961107	-210	1419.4
19961212	-175	-119
19970116	-140	255.2
19970220	-105	54.2
19970327	-70	329.9
19970501	-35	-142.5
19970605	0	0
19970710	35	42.5
19970814	70	299.7
19970918	105	-235.5
19980101	210	472
19980205	245	-29.5
19980312	280	-84.6
19980416	315	236.6
19980521	350	244.8
19980625	385	-830.1
19980730	420	341.1
19980903	455	488.7
19981112	525	565.9
19981217	560	-267.2
19990121	595	540.2
19990401	665	-181.5
19990506	700	637.1
19990610	735	232.9
19990715	770	389.8
19990819	805	1423.2

Table 2 Interferometric data used from Envisat satellite (2004-2008). Blue color indicates the master image

Date	Time interval (day)	Baseline (m)
20040603	-1190	476
20050519	-840	-77.4
20060817	-385	707.9
20060921	-350	-853.8
20061026	-315	-507.9
20070104	-245	173.2
20070208	-210	-234.9
20070315	-175	114.8
20070419	-140	-162.4
20070524	-105	-208.1
20070628	-70	-155.8
20070802	-35	-264.5
20070906	0	0
20071011	35	-346
20071115	70	63.9
20071220	105	-440
20080124	140	-193.7
20080508	245	-128.9
20080612	280	-40.5
20080821	350	-132.5
20080925	385	-281.2

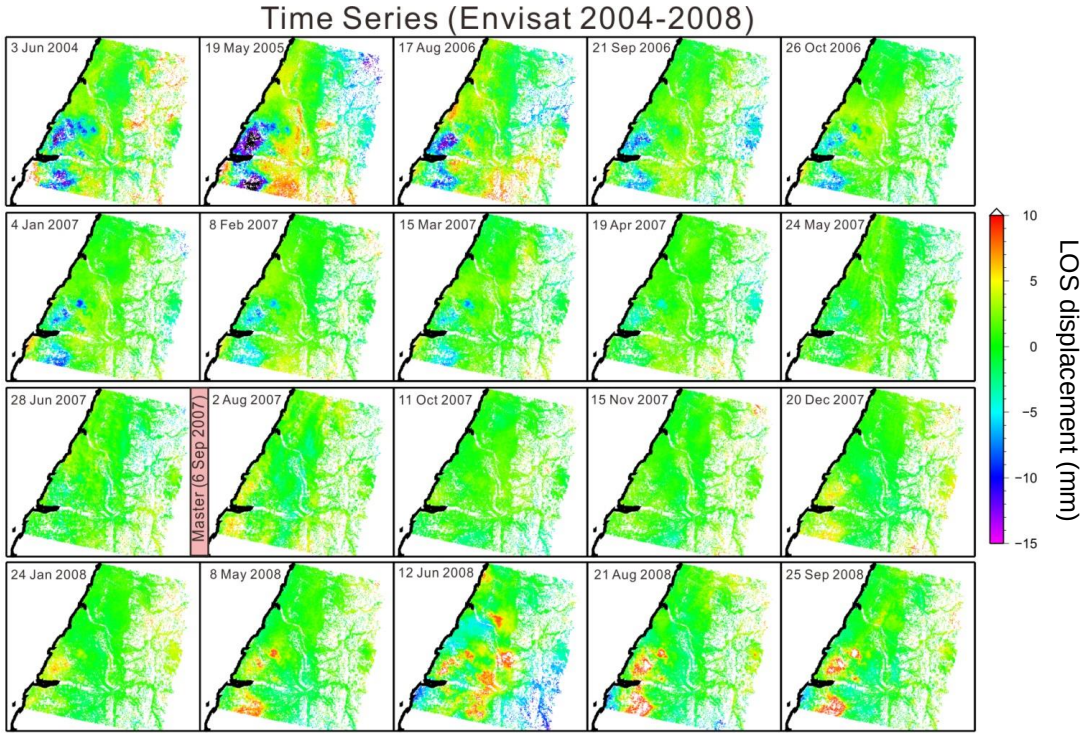

Figure 4 21 Envisat images are selected in our study. Displacements are given relative to PS pixels on 6 Sep 2007 (master image). The basins undergo a continuous process of deformation.

3.1.1 1993-1999 results (before Chi-Chi earthquake)

In Figure 5a, we show the surface deformation during preseismic period. The color represents the displacement along the LOS (line of sight) direction, where positive values (warm color) indicate relative increases in distance to the satellite, and in the other hand, the negative values (cold color) are opposite. The displacement range is about -20 ~ 0 mm/yr which are the relative values with the reference point, the CHUA GPS station showing as the red rectangular. Generally, we observed that the LOS velocity decreases from west to east comparing to the reference point. In addition to the southwest part of our study area it shows a dramatic land subsidence at Choshui alluvial fan, owing to heavy withdrawal of groundwater. It is interesting to note such geological changes in the basins and the neighboring structures, as we know, there was nearly no activity around Chelungpu fault before this Chi-Chi seismic event. Obviously, the relative lower values are shown in the basins about -10 mm/yr.

3.1.2 2004-2008 results (before Chi-Chi earthquake)

We use the same reference point (CHUA GPS station) to show the LOS velocity during postseismic period (Figure 5b). The range of the color bar is from -55 ~ 10 mm/yr which shows a larger deformation in general than the ERS result. Land subsidence in Choshui alluvial fan still shows huge decrease in the distance to the satellite. On the contrary, the footwall of the Chelungpu thrust shows apparently sustained subsidence than the hanging wall after the seismic event. Likewise, the basin region has undergone a continuing subsidence even more than the preseismic result.

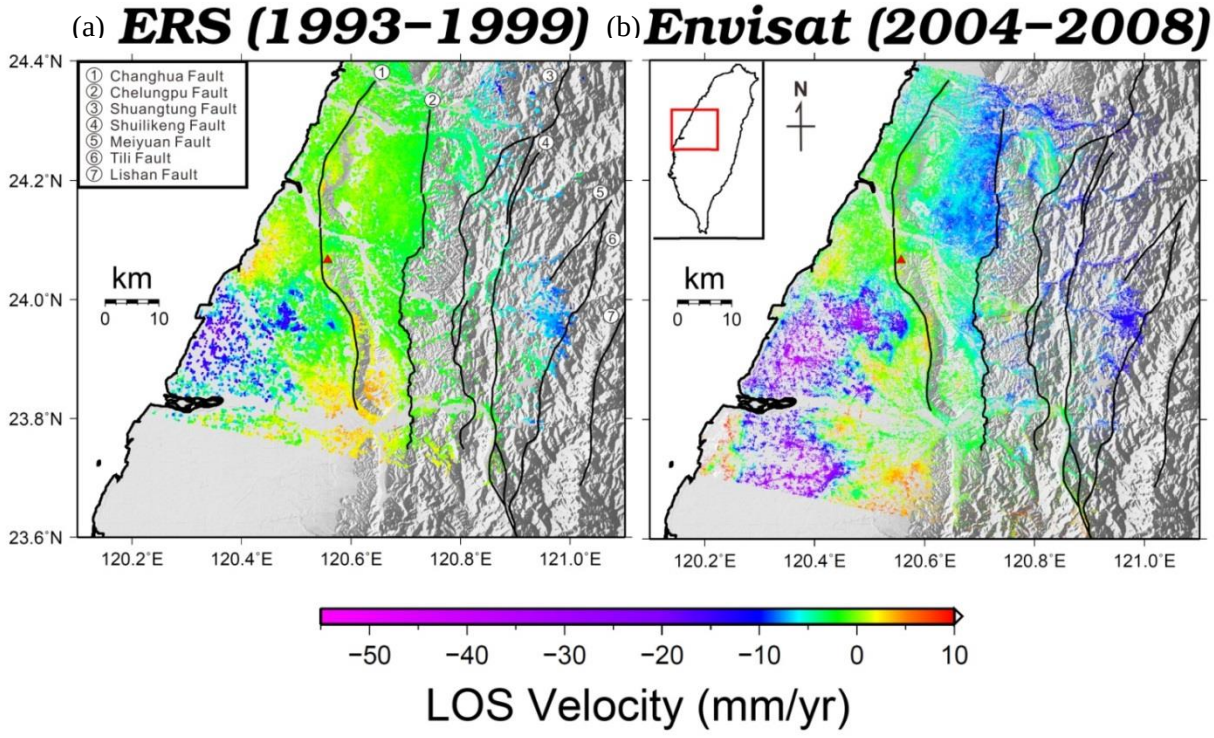

Figure 5 (a) Mean LOS velocity in 1993-1999. Black lines are the major faults in this study. Red triangular is the GPS station (CHUA) as a reference point. A relatively low LOS velocity is shown in the Puli Basin. See text for discussion and explanation. (b) Mean LOS velocity in 2004-2008. The relatively low LOS velocity is still shown in the Puli Basin after seismic event.

3.1.3 Profile analysis

In order to understand the spatial variance in displacement velocity about the basins, we draw two profiles, one oriented north-south across all the basins and one oriented east-west across the structures and Puli Basin (Figure 2).

Figure 6a shows the north-south profile, comprising both the average LOS velocity and the topography. Yellow color indicates the preseismic result, while blue color shows the velocity during postseismic period. Among these basins, Sun Moon Lake has the highest elevation but lowest velocity. Since the water has badly reflected signal which makes the result unreliable. As a whole, the basin area shows a relatively lower velocity of about -5 ~ -20 mm/yr from both periods.

Figure 6b shows the east-west profile. Red points are the location of the faults on the surface according to the structure lines from CGS. A steady velocity shows in the Changhua fault but decreases at the both side. We can observe the difference between two results of the Chelungpu fault, which shows locked before earthquake and becomes relatively low velocity area on the fault after earthquake. The trend of the LOS velocity is getting lower to the east, and the lowest value is about -15 mm/yr in the Puli Basin. Also, the postseismic result shows even lower than the preseismic one.

3.2 Dislocation models

We implemented an elastic half-space dislocation modeling software Coulomb 3.3 software (Toda *et al*., 2005; Lin *et al*., 2004) to best fit our observations of ground deformation by testing possible fault geometry and slip rates. The fault trace data are acquired from the CGS, and the parameters of the two active faults, the Changhua fault and the Chelungpu fault, are set based on previous research (Ching *et al*., 2011), whereas the rest are set by trial and error. Detail parameters corresponding to all faults in the study area are listed in Table 3. Figure 7a shows the fault geometry as a 3-dimensional from the perspective view. The ramp is set at the depth of 7~10 km west of Shuilikeng fault on the west side of Puli Basin. The east-west profile is shown in Figure 7b, where the blue dots are PSI result from 2004-2008 and the brown dots represent the motion from our best-fit model. A phenomenon we have found is that our modeled ground motion pattern can fit to our PSI observations only if a large slip rate with a westward component is set under the Puli Basin.

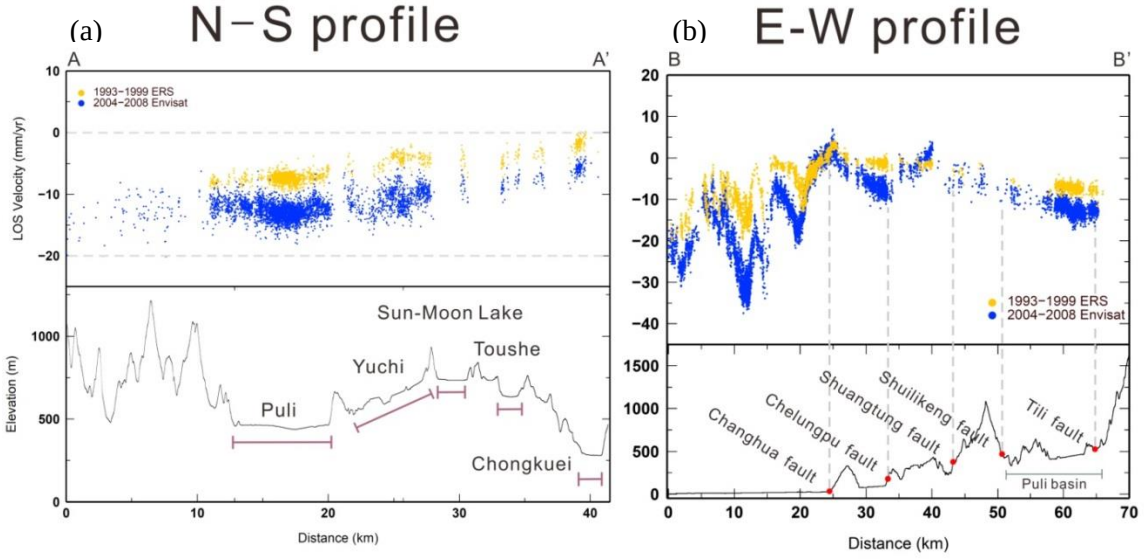

Figure 6 (a) N-S profile (A-A') of LOS velocity and the topographic profile. The locations of the profile are shown in Figure . Yellow points show the preseismic data, and the blue points show the postseismic data. (b) E-W profile (B-B') of LOS velocity and the topography. Red points are the locations of the fault on the surface from CGS geological map

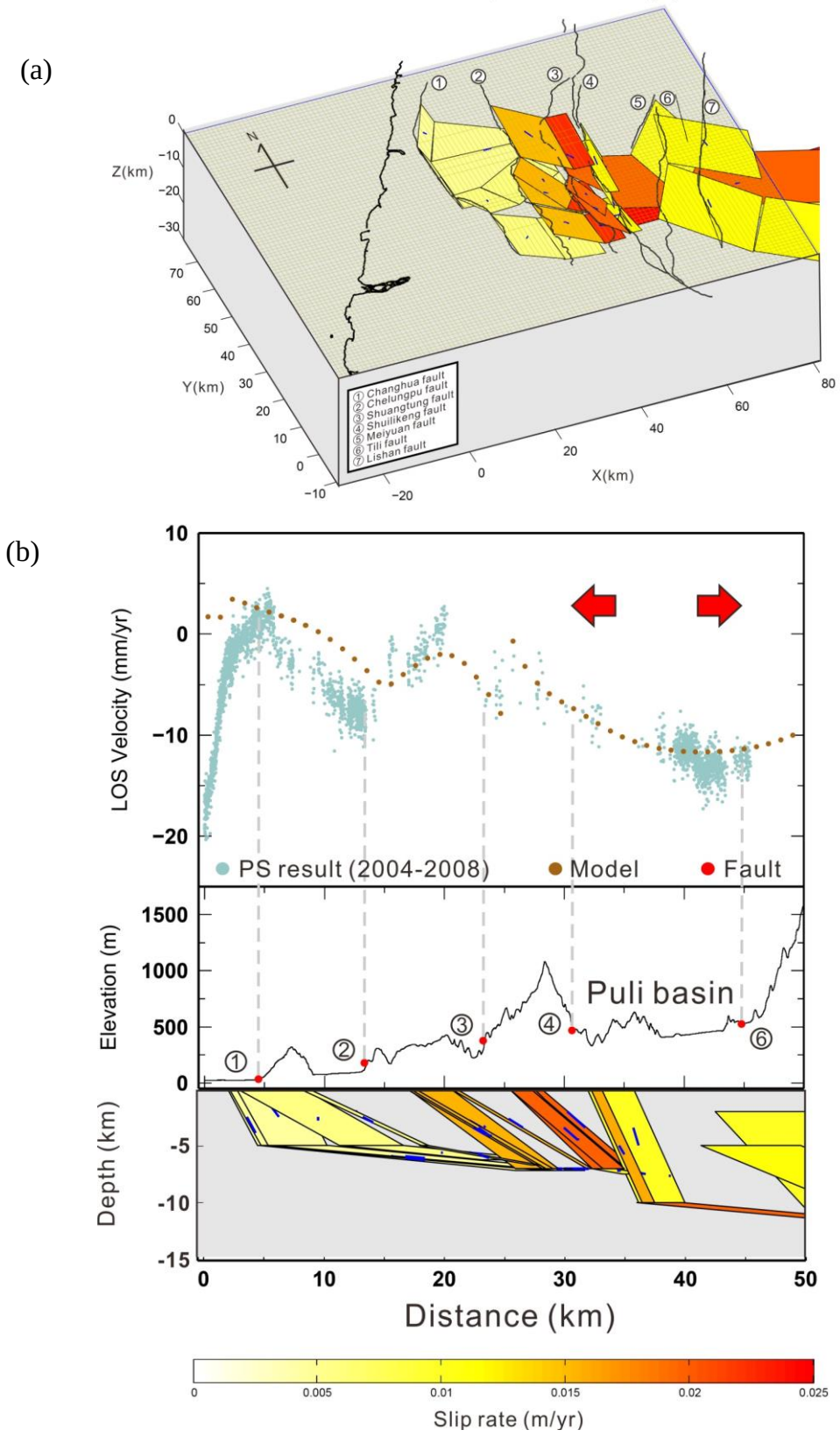

Figure 7 (a) Perspective view of our assumption model. (b) The upper diagram is the comparison of the modeling result and our PSI result (2004-2008). The lower one shows the side-look of our assumption model. The fault number is listed in Figure 7a. A ramp structure is set on the Shuilikeng fault at the depth of 10 km.

Table 3 Parameters of our assumption model

#	X-start(km)	Y-start(km)	X-fin(km)	Y-fin(km)	rt.lat(m)	Reverse(m)	dip	Top(km)	Bot(km)
1	20.6015	67.8242	14.4122	54.4748	0.0027	0.004	300	0	5
2	14.5335	54.3534	15.1403	36.9992	0.0027	0.004	300	0	5
3	15.2617	36.7564	20.9655	28.0186	0.0047	0.0037	335	0	5
4	20.7228	28.0186	21.451	12.8488	0.0047	0.0037	335	0	5
5	34.4363	61.3922	33.9509	43.0671	-0.0107	0.011	330	0	7
6	33.9509	43.3098	30.1888	38.4555	-0.011	0.011	330	0	7
7	30.0674	38.3341	30.3101	28.0186	-0.0014	0.015	330	0	7
8	30.3101	27.5332	30.9169	16.3682	-0.0014	0.015	330	0	7
9	41.9606	51.4408	41.2324	33.6011	-0.001	0.02	320	0	7
10	41.2779	33.6315	39.1693	29.839	-0.001	0.02	320	0	7
11	39.1693	30.0817	41.1111	16.975	-0.001	0.02	320	0	7
12	50.0916	49.0137	46.0868	31.6594	-0.006	0.008	295	0	10
13	46.3295	31.538	47.3003	23.0429	-0.006	0.015	295	0	10
14	68.9022	52.2903	57.2518	37.2419	-0.01	0.001	320	2	11.6
15	68.174	51.1981	64.776	34.9361	-0.01	0.005	340	5	12.5
16	64.776	34.6933	56.0382	18.4313	-0.01	0.005	340	5	12.5
17	23.2713	66.6106	17.2034	53.5039	0.0027	0.0041	355	5	7.1789
18	17.4461	54.5961	18.2956	37.2419	0.0027	0.0041	355	5	7.1789
19	24.3636	42.4603	29.9461	33.9652	0.0047	0.0037	355	5	6.3073
20	31.281	28.2613	32.1305	13.3342	0.0047	0.004	350	5	6.7365
21	46.5722	61.0282	45.9654	42.8244	-0.0107	0.02	359	7	7.0873
22	43.5382	36.0283	39.7761	31.2953	-0.0107	0.02	359	7	7.0873
23	42.5674	27.7759	43.0528	17.2177	-0.0107	0.02	359	7	7.0873
24	50.3028	51.1496	49.7944	33.0195	-0.001	0.012	350	7	7.5209
25	54.5819	47.9214	50.4557	30.6885	-0.001	0.02	355	10	15
26	51.0625	32.1448	52.0333	23.6497	-0.001	0.025	355	10	15
27	47.4223	31.2404	49.4556	18.2783	-0.001	0.012	350	7	7.5209
28	48.6084	29.546	46.5751	25.903	-0.001	0.012	350	7	7.5209
29	78.0041	45.2515	66.3536	30.2031	-0.01	0.001	355	11.6	15
30	83.4652	24.8633	74.4847	8.844	-0.01	0.005	355	12.5	15
31	42.0819	38.4555	42.9314	28.14	-0.011	0.02	359	7	7.0873

4. Discussion

4.1 Comparison with previous geodetic surveys- GPS measurement

After Chi-chi earthquake, several institutions (i.e. Central Weather Bureau (CWB), Central Geological Survey (CGS), Ministry of the Interior (MOI), the Institute of Earth Sciences of the Academia Sinica (IES), etc.) have installed continuous and campaign GPS sites in central Taiwan. In our study area, there are 69 continuous GPS (cGPS) stations and 131 campaign stations which are installed by the showing in Figure 8, and we processed data covering from January 2004 up to December 2008 from all the receivers. The analysis was carried out using GAMIT/GLOBK software, version 10.4 (Herring *et al*., 2010) to solve for daily site coordinates. The time series model that we used to calculate the motion of each site in each direction is published by Nikolaidis (2002). Then, the mean velocity of each site is estimated by weighted least square solution, and the results are provided by Crustal Deformation Research Group, National Central University. Nowadays, the accuracy of GPS velocity is about 3-5 mm for the horizontal and 6 mm for the vertical component, respectively (i.e. Larson, 1997; Borre *et al*., 2012; Steigenberger *et al*., 2012). Since GPS system measures the 3 dimensional displacement vector with components GPS_U, GPS_E and GPS_N in up, east and north directions, the feasible solution for comparison is making these components project to LOS direction. We convert GPS data into one component (GPS_{LOS}) by using the equation published by Hassen (2001):

$$GPS_{LOS} = [\cos\theta - sin\theta\ cos\alpha\ sin\theta\ sin\alpha] \begin{bmatrix} GPS_U \\ GPS_E \\ GPS_N \end{bmatrix} \quad (1)$$

where θ θ is the incidence angle which we set the average value as 23, α is the azimuth of the satellite heading vector which we set as 191.88.

Due to the distributions of GPS stations are much sparser than the PS points, we consequently use the Nearneighbor gridding algorithm in GMT to calculate the interpolated GPS results and set the same color bar with our PSI result. Both continuous and campaign GPS results show good consistency with PSI observation from 2004-2008 (Figure 8)

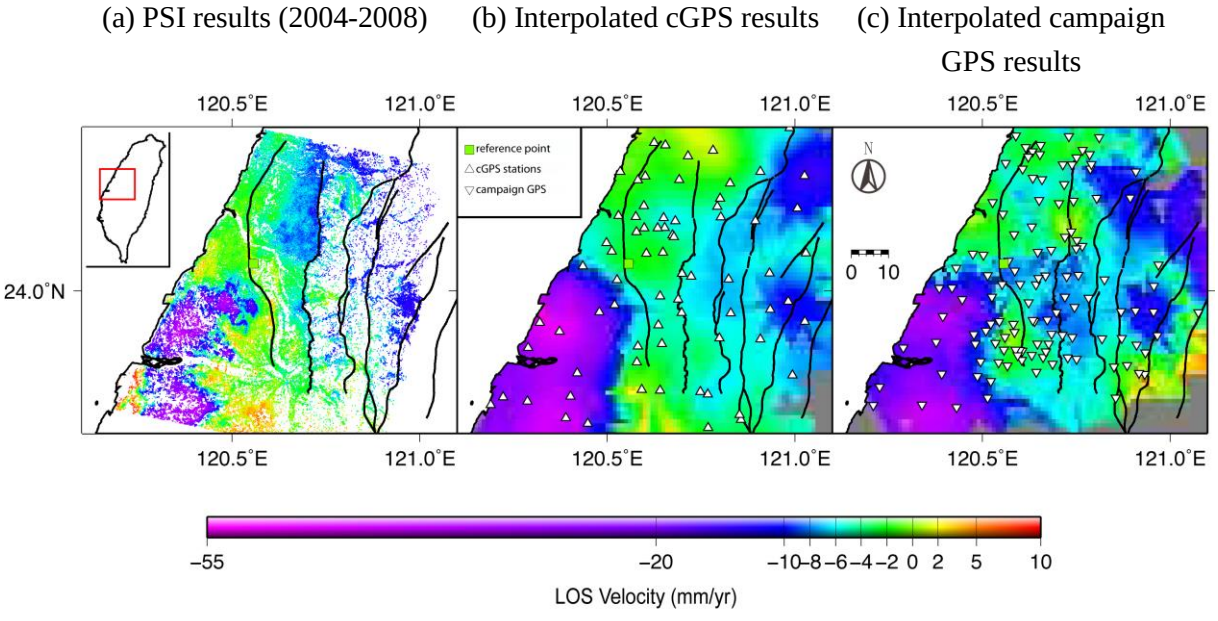

Figure 8 (a) The PSI results in 2004-2008. (b) The interpolated continuous GPS results in 2004-2008. We use 69 continuous GPS stations in our study area (yellow triangular). (c) The interpolated campaign GPS results in 2004-2008. We use 124 campaign GPS stations in our study area (black triangular)

4.2 Comparison with previous geodetic surveys-Leveling data

The leveling data from 2002-2012 are acquired from the CGS project in 2012 (Hu *et al*., 2012, in Chinese) and the average velocity results are calculated and provided by the Department of Earth Sciences, National Cheng Kung University. There are four leveling lines set and crossed the faults in our study area (Figure 9), and the accuracy of the estimation is less than 1.5 mm$\sqrt{K}$where K is the length of the survey in km) (Chou *et al*., 2008, in Chinese). We then combine the leveling data with the projected GPS measurements and our PSI result in Figure 10.

The first three results show good consistency with other geodetic surveys except the Peidou-Shuili line, which extends along the Choshui River to the east and crosses the Shuilikeng fault. In Figure 10d, an apparently opposite pattern appears in the distance of about 20~30 km. This pattern might be dominated by the horizontal component as an interpretation of my consideration. We illustrate the inconsistent part with the diagram (Figure 11). If the total GPS velocity vector shows on the left side of the dashed line, which is perpendicular to the LOS, the value shows negative when projecting to LOS such as the green arrow. In other words, we can see such opposite pattern when the horizontal component toward west is much larger than the vertical component. Since leveling data consists of vertical component only, there is no doubt that land uplift has proceeded in this region. Moreover, the GPS horizontal component shows large westward movement, and it has a same pattern when projecting to LOS (Figure 8b and Figure 8c) with our PSI result. That is, the PSI result (blue dots) and the GPS result (red and green dots) show a consistent trend in Figure 10d which makes our result to be more convincing.

4.3 Underground structure

From the PSI results, we find out that a relatively lower velocity is occurred around Puli Basin, which might be a consequence of an ongoing steep ramp structure below (Figure 7b). When combing the PSI and modeling results, we found that the geometry of the structures dominated the surface expression. That is, if the geometry of the fault is changed, the surface deformation will be different accordingly. From our results, we found two required features for the subsurface structures around the Puli Basin in order to fit the surface motion. First, a steep ramp extending eastward is possibly located at the west side of Puli Basin. Second, the slip rate on the basal detachment below Puli Basin should be relatively higher than that to the west. The abrupt slip rate change of the latter also implies the depth of the detachment may not be at the same level. The concept of the basin subsidence associated with the ramp structure effect is similar to the Chelungpu fault in Chen *et al*. (2001), while we suggest that the ramp is most likely to be formed on the Shuilikeng fault. The east part of the ramp shows subsidence and has been undergoing extension. Since the other approaches also show this characteristic (e.g. gravity survey in Ke, 2009; seismic database of Wu *et al*, (2008) in Brown *et al*, 2012). However, the basal detachment is considered to exist below the Puli Basin in order to fit with our observation, which we can observe from the seismic data as well.

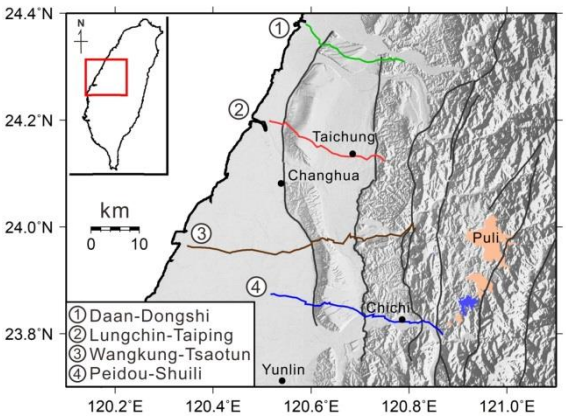

Figure 9 The location of the four leveling lines in our study area. From north to south, there are Daan-Dongshi, Lungchin-Taiping, Wangkung-Tsaotun, and Peidou-Shuili leveling line

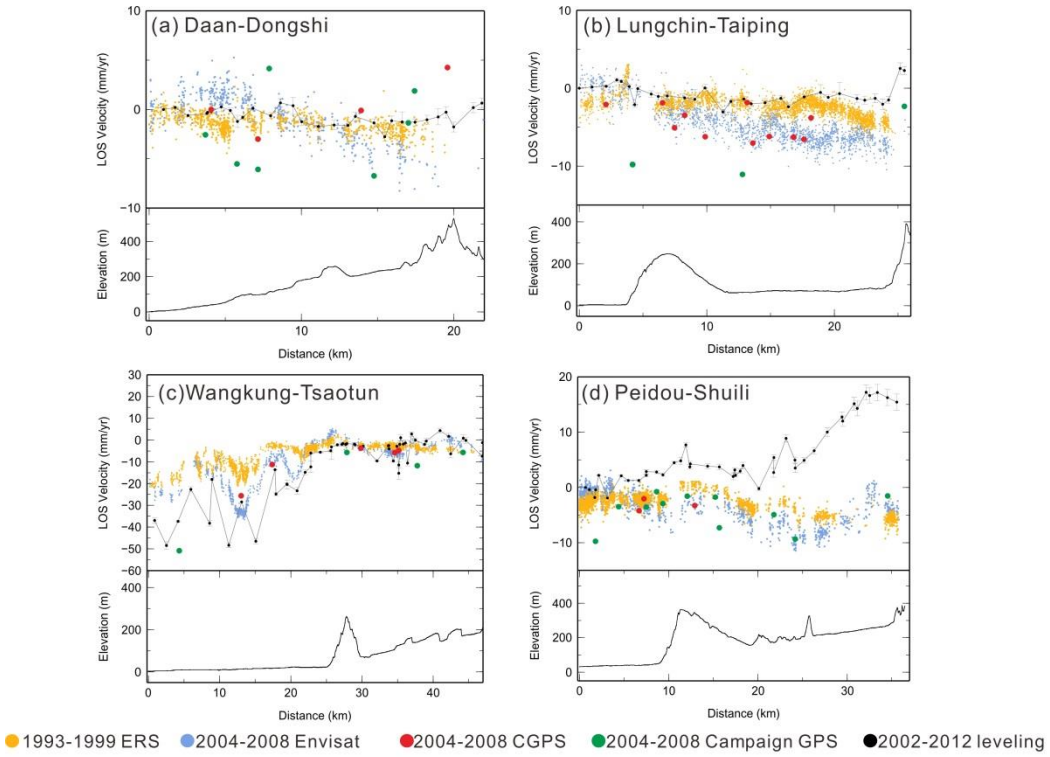

Figure 10 The upper of each diagram represents the velocity of leveling, GPS and PS results along the four leveling lines, and the lower shows the topographic profile. (a) aan-Dongshi leveling line. (b) Lungchin Taiping leveling line. (c) angkung-Tsaotun leveling line. (d) Peidou-Shuili leveling line. The explanation of the inconsistent part is discussed in Figure 11. Yellow color represents the 1993-1999 ERS results. Blue color represents the 2004-2008 Envisat results. Green and pink colors represent the continuous and campaign GPS results in 2004-2008, respectively. Black color represents the vertical velocity of leveling result in 2002-2012, and the black lines are the error bar

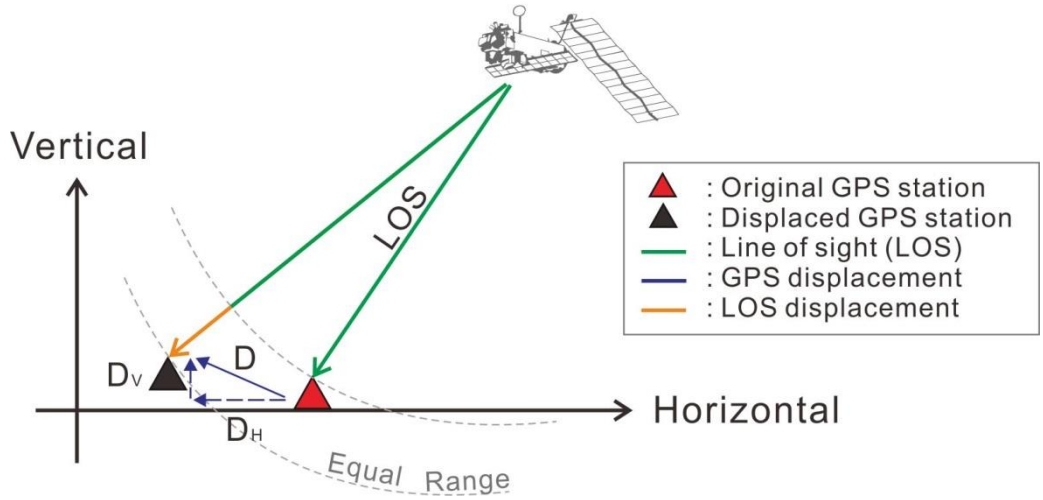

Figure 11 The illustration of the inconsistent part on Peidou-Shuili leveling line. The case for descending orbit, if the total GPS velocity vector (orange arrow) shows on the left side of the dashed line which is perpendicular to the LOS, the value shows negative when projecting to LOS such as the green arrow. See more detailed in the text

4.4 2013 Nantou earthquake series

Besides monitoring the surface deformation from the satellite, we collected the representative seismic events of central Taiwan in 2013 to show the present-day tectonic activity (2013 Nantou earthquake series). Several seismic events occurred in our study area, indicating a continuous tectonic activity on these fault zones. We take two major earthquakes in 2013 for example, one that occurred on 27 March 2013 and other that occurred on 2 June 2013. Both these events are greater than magnitude 6 on the Richter scale and belong to shallow earthquakes with focal depths less than 20 km (Figure 12d, BATS). The locations of the mainshock epicenters and the distribution of the aftershocks are shown in Figure 12. After the 2013 Nantou earthquake series, we carried out a detail field investigation in and around the epicenter area. According to our observations, the principal stress of the Changhua thrust is determined in a general east-west direction. To the east, we have observed that the Shuilikeng fault system consists of several other faults. The various directions of the stress from our field survey may be interpreted as a result from the fault movements in different periods. In the slate belt, the Lishan fault show a characteristic of both left- and right-lateral shear. In general, this region was evolving under E-W compression and N-S extension tectonic regime. Although there are no rupture and seriously deformation on the surface, we do not exclude the possible correlation between the seismic events in this region and the movement of the neighboring faults. In Figure 12c, the distribution of the aftershocks of the 0602 event is nearly horizontal beneath the mountain belt, which implies the ongoing basal detachment stretching to the east. We speculate that the detachment is linked with the Shuilikeng fault when extending to the surface and formed a ramp structure below. Also, another fault system appears at the east side of the basins, which shows an opposite strike from the aftershock distribution. It is considered to be a conjugate fault system and probably linked with Lishan fault. So far, due to the lack of evidence we cannot determine the relationship between the Lishan fault system and the mechanism of the basin subsidence. It is an interesting and worthwhile work for the further research to understand that what roles do the conjugate fault systems play during the basin subsidence.

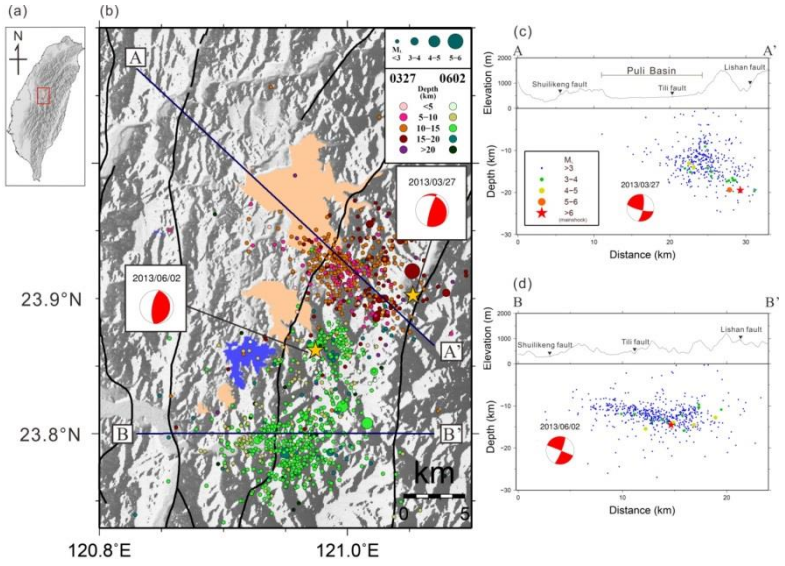

(e)

No.	Date	Time	Lat.	Long.	CWB Depth	M_L	M_w	Depth
1	20130327	02:03:19	23.9	121.07	20	6.1	5.54	15.4
2	20130602	05:43:03	23.87	121	23	6.3	5.73	10

Figure 12 (a) The distribution of both the main shock and aftershocks on 27 March (0327) and 2 June (0602), 2013 from map view. The seismicity of 0327 is in red, and the 0602 is in green. (b) The depth-distance diagram of 0327 seismicity. (c) The depth-distance diagram of 0602 seismicity (seismic data are provided from Central Weather Bureau). (d) Seismic data on 27 March and 2 June in 2013

5. Conclusion

(1) The tectonic activity and the structural features are clearly indicated from the surface expression by PSI, which is a useful technique for surface deformation monitoring.

(2) Relatively lower velocity around Puli Basin implies the depth of basal detachment changed which infers as an ongoing steep ramp structure below.

(3) PSI technique provides a comprehensive and detailed result in central Taiwan and has a good consistency with accurate GPS and leveling measurements.

(4) The distribution of aftershocks of the two events, 27 March and 2 June in 2013, showing the currently tectonic activity in the central mountain belt of Taiwan.

(5) The historical activity evidences of Shuangtung fault, Shuilikeng fault, and Lishan fault are observed in the field and shown an overall ESE-WNW principal stress direction.

On the whole, we suggest that the basin subsidence is associated with the ramp structure on the Shuilikeng fault along the basal detachment. The basins are located at the east part of the ramp, showing subsidence and have been undergoing extension. However, we suspect that the conjugate fault system is somehow related to the basin subsidence. Since a detail ground displacement data provided by the PSI has improved our understanding on fault activity in the region. It is an interesting and worthwhile work for the further research to understand more about the tectonic activity in central Taiwan.

Reference

早坂一郎，「日月潭附近山間盆地地域觀察(豫報) 」，台灣地學記事，第 1 卷，第 1 號，第 1-4 頁，1930 年。

鳥居敬造，1935，東勢地質圖幅及說明書。台灣總督府殖產局，第 732 號，共 26 頁。

陳信茂，1978，由埔里-頭社泥炭之形成探究其古地理發育。海洋彙刊，第 19 輯，第 125-130 頁。

陳炳誠，2003，埔里與魚池盆地之沈積與新構造研究，國立臺灣大學地質科學系所碩士論文，共 97 頁。

朱健仁，1991，埔里盆地群成因之探討，台灣大學地質系學士論文，共 24 頁。

楊貴三、張瑞津、沈淑敏、石同生，2007，埔里盆地的地形面，活動構造與地形演育，地理研究第 46 期，共 16 頁。

周侑德、景國恩、饒瑞鈞、劉啟清，2008，精密水準觀測之資料品質及精度分析，經濟部中央地質調查所特刊，第 20 號，第 49-62 頁。

黃慶甲，2008，以淺層反射震測探勘埔里盆地地下構造，國立中央大學地球物理所碩士論文。

柯展，2009，台中-埔里重力低區之研究，國立中央大學地球物理所碩士論文。

柯瑞祥，2009，埔里盆地之震測研究，國立中央大學地球物理所碩士論文，共 78 頁。

胡植慶、劉啟清、饒瑞鈞、李元希、鄭錦桐、張午龍、陳卉瑄、景國恩、唐昭榮，2012，地調所「斷層活動性觀測研究第二階段-斷層監測與潛勢分析研究」計畫總報告，共 856 頁。經濟部中央地質調查所，新北。

Biq, C., 1989, The Yushan-Hsuehshan megashear zone in Taiwan: in Proceedings Proc. Geol. Soc. China, v. 32, p. 7-20.

Borre, K., and Strang G., 2012, Algorithms for global positioning: Wellesley-Cambridge Press.

Brown, D., Alvarez-Marron, J., Schimmel, M., Wu, Y.-M., and Camanni, G., 2012, The structure and kinematics of the central Taiwan mountain belt derived from geological and seismicity data: Tectonics, v. 31, no. 5, pp 25.

Chapple, W. M., 1978, Mechanics of thin-skinned fold-and-thrust belts: Geological Society of America Bulletin, v. 89, no. 8, p. 1189-1198.

Chang, C.-P., Angelier, J., and Lu, C.-Y., 2009, Polyphase deformation in a newly emerged accretionary prism: Folding, faulting and rotation in the southern Taiwan mountain range: Tectonophysics, v. 466, p. 395-408.

Chang, C.-P., Yan, J.-Y, Hooper, A., Chou, F.-M., Chen, Y.-A., Hou, C.-S., Hung, W.-C., Lin, M.-S., 2010, Monitoring of Surface

Deformation in Northern Taiwan Using DInSAR and PSInSAR Techniques: Terr. Atmos. Ocean. Sci., v. 21, no. 3.

Chen, W.-S., Huang, B.-S., Chen, Y.-G., Lee, Y.-H., Yang, C.-N., Lo, C.-H., Chang, H.-C., Sung, Q.-C., Huang, N.-W., and Lin, C.-C., 2001, 1999 Chi-Chi Earthquake: A Case Study on the Role of Thrust-Ramp Structures for Generating Earthquakes: Bulletin of the Seismological Society of America, v. 91, no. 5, p. 986-994.

Ching, K.-E., Rau, R.-J., Johnson, K. M., Lee, J.-C., and Hu, J.-C., 2011, Present-day kinematics of active mountain building in Taiwan from GPS observations during 1995–2005: J. Geophys. Res., v. 116, no. B9.

Dahlen, F., Suppe, J., and Davis, D., 1984, Mechanics of fold-and-thrust belts and accretionary wedges: Cohesive Coulomb theory: J. Geophys. Res.: Solid Earth, v. 89, no. B12, p. 10087-10101.

Davis, D., Suppe, J., and Dahlen, F., 1983, Mechanics of fold-and-thrust belts and accretionary wedges: J. Geophys. Res.: Solid Earth (1978–2012), v. 88, no. B2, p. 1153-1172.

Hanssen, R. F., 2001, Radar interferometry: data interpretation and error analysis: Springer, v5.

Herring, T. A., King R. W., and McClusky S. C., 2010, Introduction to GAMIT/GLOBK Version 10.4, Massachusetts Institute of Technology, Cambridge.

Ho, C.-S., 1986, A synthesis of the geologic evolution of Taiwan: Tectonophysics, v. 125, no. 1, p. 1-16.

Ho, C.-S., 1982, Tectonic evolution of Taiwan - Explanatory text of the tectonic map of Taiwan: Ministry of Economic Affairs, R.O.C., p. 1-126

Hooper, A., 2004, A new method for measuring deformation on volcanoes and other natural terrains using InSAR persistent scatterers: Geophysical Research Letters, v. 31, no. 23.

Hooper, A., Segall P., and Zebker H., 2007, Persistent scatterer interferometric synthetic aperture radar for crustal deformation analysis, with application to Volca´n Alcedo, Gala´pagos: J. Geophys. Res., v. 112, no. B07407.

Larson, K. M., Freymueller J. T., Philipson S., 1997, Global plate velocities from the Global Positioning System: J. Geophys. Res., v. 102, pp. 9961–9981.

Lin, J., and Stein, R.-S., 2004, Stress triggering in thrust and subduction earthquakes and stress interaction between the southern San Andreas and nearby thrust and strike-slip faults: J. Geophys. Res.: Solid Earth, v. 109, no. B2.

Mueller, K., Y. Chen, and L. Powell, 2002, Modern strain and structural architecture of the central Taiwanese orogen: Evidence for active backstepping in response to erosion?, Eos Trans. AGU, 83(47), Fall Meet. Suppl., Abstract T61B-1279.

Nikolaidis, R., 2002, Observation of geodetic and seismic deformation with the Global Positioning System. Ph.D. dissertation, Univ. of Calif., San Diego, La Jolla.

Powell, L., K. Mueller, and Y. Chen, 2002, Geomorphic constraints on patterns of shortening and erosion in the Puli Basin: Hinterland of the central Taiwan Thrust Belt, Eos Trans. AGU, 83(47), Fall Meet. Suppl., Abstract T61B-1270.

Steigenberger P., Seitz M., Böckmann S., Tesmer V., Hugentobler, U. ,2012, Precision and Accuracy of GPS-derived Station Displacements: Physics and Chemistry of the Earth, v. 53-54, pp. 72-79

Stockmal, G. S., 1983, Modeling of large-scale accretionary wedge formation, J. Geophys. Res., v. 88, pp. 8271–8287.

Suppe, J., 1983, Geometry and kinematics of fault-bend folding: Amer. Jour. Sci., v. 283, p. 684-721. [Reprinted in Amer. Assoc. Petroleum Geol., Treatise of Petroleum Geology, Reprint Series no. 9, N.H. Foster and E.A. Beaumont, eds., Structural Concepts and Techniques II., p. 422-461.]

Toda, S., Stein, R. S., Richards-Dinger, K., and Bozkurt, S. B., 2005, Forecasting the evolution of seismicity in southern California: Animations built on earthquake stress transfer: J. Geophys. Res., v. 110, no. B5, p. B05S16.

Van der Pluijm, B. A., and Marshak, S., 2004, Earth structure: An introduction to

structural geology and tectonics(2nd edition): New York, W.W. Norton, 656p.

Wu, Y.-M., Zhao, L., Chang, C.-H., and Hsu, Y.-J., 2008, Focal-mechanism determination in Taiwan by genetic algorithm: Bulletin of the Seismological Society of America, v. 98, no. 2, p. 651-661.

Yanites, B. J., Tucker, G. E., Mueller, K. J., Chen, Y.-G., Wilcox, T., Huang, S.-Y., and Shi, K.-W., 2010, Incision and channel morphology across active structures along the Peikang River, central Taiwan: Implications for the importance of channel width: Geological Society of America Bulletin, v. 122, no. 7-8, p. 1192-1208.

Yue, L.-F., Suppe, J., and Hung, J.-H., 2005, Structural geology of a classic thrust belt earthquake: the 1999 Chi-Chi earthquake Taiwan (Mw=7.6): J. Geophys. Res., v. 27, no. 11, p. 2058-2083.

台灣中部埔里盆地的構造活動：衛星遙測和野外觀測

許庭瑄[1] 張中白[2*] 張午龍[3]

摘 要

埔里盆地位於西部麓山帶和雪山山脈之間，是台灣活躍造山帶中面積最大的山間盆地。埔里盆地，與其南邊一系列沿北北東走向分佈的小盆地的發育和地下構造應有密切相關，綜合許多前人研究所提出用以闡釋埔里盆地群形成之構造模型，本研究推測此處應為一構造運動的轉變帶。本研究以衛星雷達量測地表變形，配合野外調查以瞭解及分析埔里盆地及周圍地區的構造及其活動特性。本研究使用永久散射體差分干涉技術用以監測地殼變形，結果顯示埔里盆地的衛星視角速度相對其他地區較低，表示埔里盆地的運動方向正遠離衛星，這可能代表盆地西側的滑脫面上有一斷坡構造，滑脫面在盆地下方有向下變深的現象，使得地表的運動方向有所改變。為了解釋台灣中部地表變形的機制，我們以前人研究的構造模型為依據，利用模型正演來檢視地下構造和地表變形的關係，並逐一討論之。本研究亦將衛星觀測結果與全球衛星定位系統和精密水準測量資料結合，並配合野外調查了解構造實際出露位置及其活動特性，初步結果推測埔里盆地是由於滑脫帶上的斷坡構造活動時造成盆地相對陷落。此外，由 2013 年 3 月 27 日及 6 月 2 日的南投地震及其餘震分布可以發現盆地下方除了滑脫構造面外，還存在和另一共軛的斷層系統，初步推測此共軛斷層系統和埔里盆地群的形成有一定的關連，為未來值得深入研究的主題。

關鍵詞：構造活動、埔里盆地、永久散射法雷達差分干涉技術、錯位模型、野外調查

[1] 國立中央大學地球科學系 碩士
[2] 國立中央大學太空及遙測研究中心 教授
[3] 國立中央大學地球科學系 副教授
*通訊作者, 電話: 03-4227151 ext.57627，E-mail: cpchang@csrsr.ncu.edu.tw

收到日期:民國 102 年 11 月 08 日
修改日期:民國 103 年 08 月 17 日
接受日期:民國 103 年 08 月 27 日